

Blowout bifurcation and on-off intermittency in pulse neural networks with multiple modules

Takashi Kanamaru

Department of Basic Engineering in Global Environment,
Faculty of Engineering, Kogakuin University,
2665-1 Nakano, Hachioji-city, Tokyo 192-0015, Japan

International Journal of Bifurcation and Chaos, vol.16, no.11 (2006) pp.3309-3321.

Abstract

To study the mechanism by which high-dimensional chaos emerges in neural systems, the synchronization of chaotic firings in class 1 pulse neural networks composed of excitatory and inhibitory ensembles was analyzed. In the system with two modules (*i.e.*, two pulse neural networks), blowout bifurcation and on-off intermittency were observed when the inter-module connection strengths were reduced from large values. In the system with three modules, rearrangement of synchronized clusters and chaotic itinerancy were observed. Such dynamics may be one of the mechanisms through which high-dimensional chaos is generated in neural systems.

1 Introduction

Since the 1980s, many efforts have been made to elucidate the chaotic dynamics in neural systems. Chaotic dynamics were observed *in vitro* in single neurons such as the squid giant axon [Matsumoto *et al.*, 1984] and the onchidium giant neuron [Hayashi *et al.*, 1982]. Chaotic dynamics were also observed in neuronal networks such as the olfactory bulb of rabbits [Freeman, 1987]. Although chaotic dynamics were demonstrated in experimental studies, it is unclear whether chaotic dynamics actually exist in neural systems under normal conditions. It is also unclear whether chaotic dynamics are useful in information processing in neural systems.

On the other hand, in modeling studies, it was reported that chaotic dynamics were useful in some neural dynamics such as the escape from local minima in optimization problems and the chaotic transition among memory states in associative memory models [Aihara *et al.*, 1990; Inoue & Nagayoshi, 1991; Nara & Davis, 1992; Tsuda, 1992; Adachi & Aihara, 1997; Uchiyama & Fujisaka, 2004]. Such chaotic dynamics might be related to chaotic itinerancy [Kaneko & Tsuda, 2000], which is frequently discussed in high-dimensional chaotic systems. Such high-dimensional chaotic dynamics were realized in networks of artificial models of neurons; therefore, it

is important to confirm that high-dimensional chaos can be observed in more realistic pulse neural networks. Although it was reported that single pulse neurons [Feudel *et al.*, 2000; Varona *et al.*, 2001] and pulse neural networks [van Vreeswijk & Sompolinsky, 1996; Kanamaru & Sekine, 2005] can show chaotic behaviors, they were low-dimensional chaos, and it was not known whether neural systems show high-dimensional chaos. Chaotic itinerancy in pulse neural networks was previously reported in networks of four or five Bonhöffer-van der Pol neurons by Tsumoto *et al.* [2002]. However, they stated that only a very narrow range of values for the parameters resulted in chaotic itinerancy in their model, and it was unclear whether chaotic itinerancy could be observed in networks consisting of many neurons.

To obtain high-dimensional chaos, the theory of synchronization of chaos can be applied. When two systems that each shows low-dimensional chaos, are diffusively coupled and when their coupling strengths are strong enough, these two systems perfectly synchronize with each other on a low-dimensional chaotic attractor. When the coupling strengths are reduced, blowout bifurcation [Ott & J.C. Sommerer, 1994] occurs and this synchronization of chaos is broken. The synchronization of chaos is interpreted as confinement of the coupled system in an invariant manifold, and the blowout bifurcation destabilizes this invariant manifold along the direction transverse to the manifold; therefore, the dimension of chaos increases if there are no other attractors. Diffusive coupling is realized by electrical synapses in neural systems [Nicholls *et al.*, 2001], and synchronization of chaos and its destabilization are observed in pulse neural networks that are connected by electrical synapses [Elson *et al.*, 1998; Yoshioka, 2005]. However, it is thought that chemical synapses are more frequent than electrical synapses in the brain. It is unknown whether blowout bifurcation occurs in a network of neurons that are connected by chemical synapses. It is also unknown how high-dimensional chaos is realized with chemical synapses.

In the present study, in order to elucidate the mechanism by which high-dimensional chaos emerges in neural systems, we examine the chaotic dynamics in pulse

neural networks of neurons that are connected by chemical synapses. In Sec.2, we define a module of a pulse neural network that is composed of an ensemble of excitatory neurons and an ensemble of inhibitory neurons. To analyze the dynamics of this one-module system, we performed linear analyses around the equilibrium points with the Fokker-Planck equation, and various synchronized firings are observed depending on the values of the parameters including noise intensity and the connection strengths [Kanamaru & Sekine, 2005]. In Sec.3, we focus on a set of values of the parameters in which the neurons in a one-module system show synchronized chaotic firings with a low-dimensional attractor, and we analyze the inter-module synchronization between two modules of networks. We found that the inter-module synchronization of chaotic firings was stable when the connection strength was large, but when the connection strength was reduced, the inter-module synchronization of chaotic firings became unstable. It was found that this transition was caused by blowout bifurcation [Ott & Sommerer, 1994]. Behavior typical of the on-off intermittency [Fujisaka & Yamada, 1986; Heagy *et al.*, 1994; Hata & Miyazaki, 1997] was also observed. The inter-module synchronization of chaotic firings and its destabilization caused rearrangements of synchronized clusters and chaotic itinerancy. In Sec.4, tests on Morris-Lecar neurons are performed, and similar chaotic dynamics are observed. The final section provides a discussion and conclusions.

2 One-Module System

In this section, we study a pulse neural network composed of an ensemble of excitatory neurons with internal states $\theta_E^{(i)}$ ($i = 1, 2, \dots, N_E$) and an ensemble of inhibitory neurons with internal states $\theta_I^{(i)}$ ($i = 1, 2, \dots, N_I$) that are written as

$$\begin{aligned} \dot{\theta}_E^{(i)} &= (1 - \cos \theta_E^{(i)}) + (1 + \cos \theta_E^{(i)}) \\ &\quad \times (r_E + \xi_E^{(i)}(t) + g_{EE}I_E(t) - g_{EI}I_I(t)), \end{aligned} \quad (1)$$

$$\begin{aligned} \dot{\theta}_I^{(i)} &= (1 - \cos \theta_I^{(i)}) + (1 + \cos \theta_I^{(i)}) \\ &\quad \times (r_I + \xi_I^{(i)}(t) + g_{IE}I_E(t) - g_{II}I_I(t)), \end{aligned} \quad (2)$$

$$I_X(t) = \frac{1}{2N_X} \sum_{i=1}^{N_X} \sum_j \frac{1}{\kappa_X} \exp\left(-\frac{t-t_j^{(i)}}{\kappa_X}\right), \quad (3)$$

$$\langle \xi_X^{(i)}(t) \xi_Y^{(j)}(t') \rangle = D \delta_{XY} \delta_{ij} \delta(t-t'), \quad (4)$$

where $X, Y = E$ or I . Note that g_{XY} is the connection strength from ensemble Y to ensemble X , δ_{XY} and δ_{ij} are Kronecker's deltas, and $t_j^{(i)}$ is the j -th firing time of the i -th neuron in ensemble X , which will be defined later. $I_X(t)$ is the synaptic inputs from ensemble X to the other ensemble in which the neurons are connected by chemical synapses, and $\xi_X^{(i)}(t)$ is the noise in the i -th neuron in ensemble X . Note that the second sum in the

definition of $I_X(t)$ is taken over j satisfying $t > t_j^{(i)}$. In the following, we call this network with excitatory and inhibitory ensembles as the one-module system.

In the absence of noise $\xi_X^{(i)}(t)$ and synaptic inputs $I_X(t)$, a single neuron shows self-oscillation when the system parameter r_X satisfies $r_X > 0$. When $r_X < 0$, this neuron becomes an excitable system with a stable equilibrium written by

$$\theta_0 = -\arccos \frac{1+r_X}{1-r_X}, \quad (5)$$

in which θ_0 is close to zero for $r_X \sim 0$. We define the firing time of the neuron as the time at which $\theta_X^{(i)}$ exceeds π because π is greatly differs from θ_0 (~ 0). In the following, we use values of the parameter where $r_X < 0$ and we consider the dynamics of the networks of excitable neurons.

Note that the synaptic input $I_X(t)$ from ensemble X can be rewritten as

$$I_X(t) = \frac{1}{N_X} \sum_{i=1}^{N_X} I_X^{(i)}(t), \quad (6)$$

$$I_X^{(i)}(t) = -\frac{1}{\kappa_X} \left(I_X^{(i)}(t) - \delta(\theta_X^{(i)} - \pi) \right), \quad (7)$$

and the system governed by Eqs. (1), (2), (6), and (7) has the form of the canonical model of slowly connected class 1 neurons [Izhikevich, 1999, 2000]. Thus, the network of slowly connected arbitrary class 1 neurons [Ermentrout, 1996; Izhikevich, 1999] with global connections can be transformed into the above form with the appropriate change of variables. Here we restrict the parameters so that the system parameters r_E and r_I and the noise intensity D are uniform in the network. Moreover, we introduce the internal connection strength g_{int} in an ensemble and the external connection strength g_{ext} between ensembles, and the restrictions $g_{EE} = g_{II} \equiv g_{int} = 4$ and $g_{EI} = g_{IE} \equiv g_{ext}$ are placed on the connection strengths for simplicity. In the following, the parameters are set at $r_E = -0.025$, $r_I = -0.025$, and $\kappa_E = \kappa_I = 1.0$.

Let us analyze the synchronized firings observed in the one-module system. The dynamics of the one-module system are nearly identical with the dynamics of the exponentially coupled active rotators analyzed by Kanamaru & Sekine [2005]. Therefore, we will provide a brief description here. In the limit of $N_E, N_I \rightarrow \infty$, the average behavior of the neurons in the system can be analyzed with the Fokker-Planck equations, which are shown in Appendix A. Figure 1(a) shows a bifurcation set that had been obtained numerically by the method described in Appendix B. Figure 1(b) shows the probability fluxes in the (J_E, J_I) plane of the regions indicated by Roman numerals in the bifurcation set in Fig. 1(a). The probability fluxes J_E and J_I at $\theta = \pi$ are defined in Appendix A. Note that J_E and J_I can be interpreted as the instantaneous average firing rates of the excitatory and

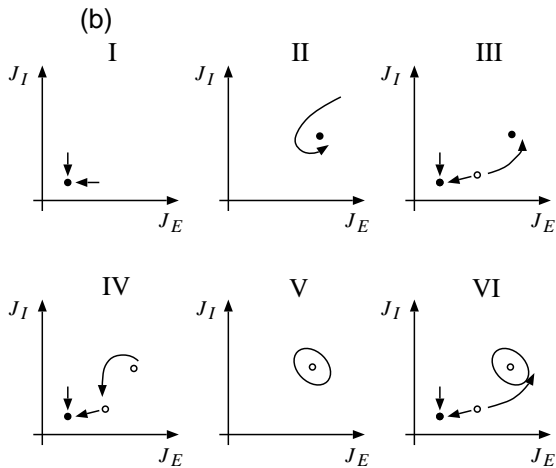
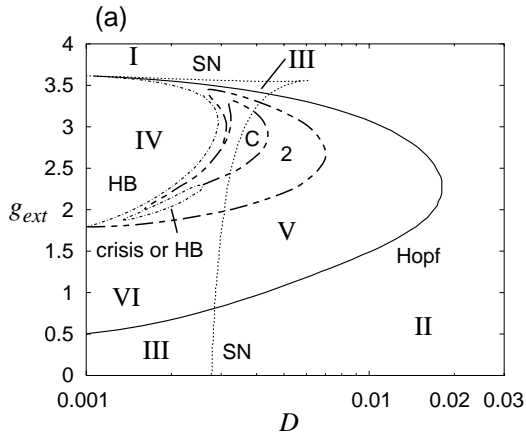


Figure 1: (a) A bifurcation set in the (D, g_{ext}) plane. D and g_{ext} denote the noise intensity and the external connection strength, respectively. The solid, dotted, and dash-dotted lines denote the Hopf, saddle-node, and homoclinic bifurcations, respectively. The areas where the periodic solution with cycle 2 or the chaotic solution exists are roughly sketched. SN, saddle-node; HB, homoclinic bifurcation. (b) Schematic flows of the solution in various regions in the (J_E, J_I) plane are shown. The filled and open circles denote the stable and unstable equilibrium points, respectively. The solid closed curves denote the stable limit cycle.

inhibitory ensembles, respectively. When the probability fluxes converge to an equilibrium point, all neurons fire asynchronously, and when the probability fluxes converge to a time-varying solution, there are some correlations among the firings of neurons.

Let us understand the bifurcation set in Fig. 1(a) using the schematic flows in Fig. 1(b). For a large noise intensity D , there exists only one equilibrium point with large firing rates, as shown in the schematic flow for region II in Fig. 1(b). This equilibrium point corresponds to the state where all neurons fire with large firing rates without correlations among them. When this equilibrium point loses stability through the Hopf bifurcation,

a limit cycle that corresponds to synchronized firings appears. Note that as g_{ext} increases, this equilibrium point approaches the origin of the (J_E, J_I) plane. Thus, the schematic flow for region II smoothly changes to the flow for region I. When the noise intensity D is small, there exists a stable equilibrium point that is close to the origin, as shown in the schematic flows for regions I, III, and IV. This equilibrium point corresponds to the state where all neurons are fluctuating around their equilibria because of the small D . When a homoclinic bifurcation takes place near this stable equilibrium point, a limit cycle appears and neurons start to fire synchronously.

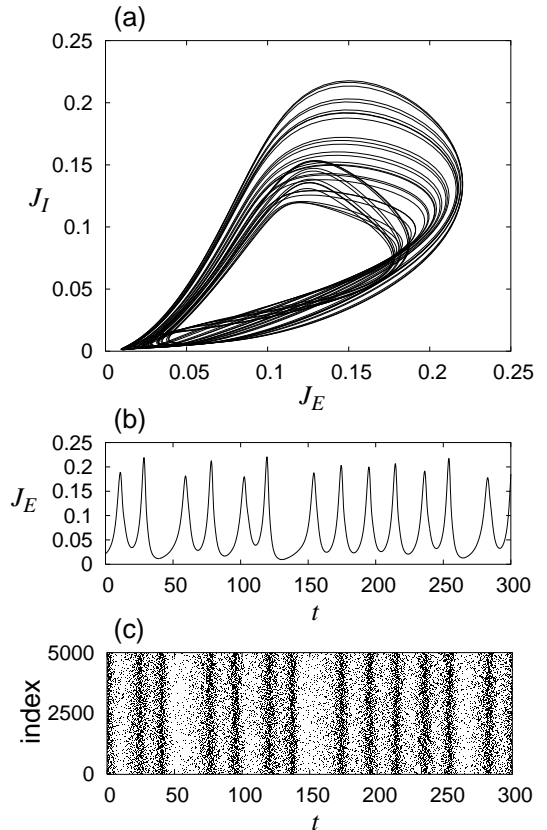


Figure 2: One-module system where $D = 0.0042$, $g_{int} = 4$, and $g_{ext} = 2.8$. (a) Chaotic flow in the (J_E, J_I) plane. (b) Change in J_E over time. (c) Raster plot of the firing times of the excitatory neurons in the system with $N_E = N_I = 5000$.

In addition to the above bifurcations, there also exist a series of period doubling bifurcations and chaotic dynamics in the one-module system. The area where the periodic solution with cycle 2 exists and the area where the chaotic solution exists, are roughly sketched in Fig. 1(a), and they are labeled as “2” and “C”, respectively. Although periodic solutions with higher cycles also exist, these areas were omitted from Fig. 1(a) because they were very narrow. An example of the chaotic dynamics in a one-module system where $D = 0.0042$, $g_{int} = 4$, and $g_{ext} = 2.8$ is shown in Fig. 2. The chaotic flow in

the (J_E, J_I) plane and the change in J_E over time are shown in Figs. 2(a) and 2(b), respectively. A chaotic attractor is observed in Fig. 2(a). The firing times of the excitatory neurons in the one-module system with $N_E = N_I = 5000$ are shown in Fig. 2(c). It is observed that the interval between the synchronized firings fluctuates chaotically.

Figure 3(a) shows a graph of the position of the attractor on the Poincaré section $J_E = 0.125$ with $J_E/dt > 0$ against the noise intensity D . Period-doubling bifurca-

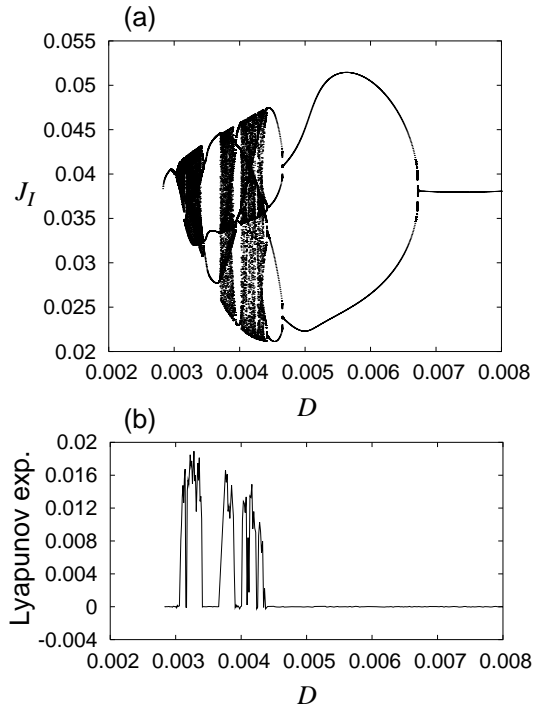


Figure 3: (a) Position of the attractor on the Poincaré section $J_E = 0.125$ with $J_E/dt > 0$ against D for $g_{int} = 4$ and $g_{ext} = 2.8$. (b) Dependence of the largest Lyapunov exponent on the noise intensity D .

tions and chaotic dynamics are observed. The largest Lyapunov exponent was calculated by the method described in Appendix B, and its dependence on the noise intensity D is shown in Fig. 3(b). It is observed that the largest Lyapunov exponent assumes positive values where there are chaotic dynamics.

The phenomenon observed in this section can be regarded as an example of noise-induced complexity [Lindner *et al.*, 2004; Zaks *et al.*, 2005] and, more specifically, coherence resonance [Pikovsky & Kurth, 1997; Zhou *et al.*, 2001]. As the noise intensity D increases from 0.001, a periodic solution appears in the present model and then it disappears as the noise intensity increases further (Fig. 1(a)). This result is similar to that obtained in our previous analysis of array-enhanced coherence resonance [Kanamaru & Sekine, 2003]. Thus, the periodicity of the output of the system would be maximized at an optimal noise intensity. However, chaotic solutions also exist in

the present model; therefore, careful analyses were required.

The chaotic attractor observed in Fig. 2(a) is low-dimensional because the number of positive Lyapunov exponents was only one. We are interested in high-dimensional chaos, because it is believed that the chaotic dynamics that are useful in information processing are high-dimensional [Aihara *et al.*, 1990; Inoue & Nagayoshi, 1991; Nara & Davis, 1992; Tsuda, 1992; Adachi & Aihara, 1997; Uchiyama & Fujisaka, 2004]. However, it is not known how high-dimensional chaos is realized in a network of neurons that are connected by chemical synapses. In the next section, we study networks consisting of multiple modules to examine the possibility of the presence of high-dimensional chaos in the neural system.

3 M -Module System

In this section, to elucidate the mechanism through which high-dimensional chaos emerges in neural systems, we study the M -module system in which the internal states of the neurons are defined as:

$$\begin{aligned} \dot{\theta}_{E_k}^{(i)} &= (1 - \cos \theta_{E_k}^{(i)}) + (1 + \cos \theta_{E_k}^{(i)}) \\ &\quad \times (r_{E_k} + \xi_{E_k}^{(i)}(t) + g_{E_k E_k} I_{E_k}(t) - g_{E_k I_k} I_{I_k}(t) \\ &\quad + \sum_{l \neq k} (\epsilon_{E_k E_l} I_{E_l}(t) - \epsilon_{E_k I_l} I_{I_l}(t))), \end{aligned} \quad (8)$$

$$\begin{aligned} \dot{\theta}_{I_k}^{(i)} &= (1 - \cos \theta_{I_k}^{(i)}) + (1 + \cos \theta_{I_k}^{(i)}) \\ &\quad \times (r_{I_k} + \xi_{I_k}^{(i)}(t) + g_{I_k E_k} I_{E_k}(t) - g_{I_k I_k} I_{I_k}(t) \\ &\quad + \sum_{l \neq k} (\epsilon_{I_k E_l} I_{E_l}(t) - \epsilon_{I_k I_l} I_{I_l}(t))), \end{aligned} \quad (9)$$

where $k = 1, 2, \dots, M$ and represents the index of the modules. For simplicity, we set the intra-module connection strengths as $g_{X_k Y_k} = g_{XY}$ and the inter-module connection strengths as $\epsilon_{X_k Y_l} \equiv \epsilon_{XY} (k \neq l)$. In the following, we examine the inter-module synchronization of chaotic firings in this M -module system.

First, we consider a two-module system. Let us introduce a set of intra-module connection strengths g_{int}^* and g_{ext}^* with which the neurons in a one-module system show synchronized chaotic firings with a low-dimensional attractor, *e.g.*, $g_{int}^* = 4$ and $g_{ext}^* = 2.8$, as shown in Fig. 2. When two modules of networks with g_{int}^* and g_{ext}^* are connected, these modules do not show inter-module synchronization of chaotic firings, but converge to a periodic solution (data not shown) because the connections are not diffusive but are synaptic with chemical synapses, as shown in Eq. (3). In order to obtain inter-module synchronization of chaotic firings, we introduce an arrangement of connection strengths as shown in Fig. 4; namely, for ϵ_{EE} and ϵ_{IE} , the intra-module connection strengths are set as $g_{EE} = g_{int}^* - \epsilon_{EE}$, $g_{II} = g_{int}^*$, $g_{IE} = g_{ext}^* - \epsilon_{IE}$, and $g_{EI} = g_{ext}^*$. Note that the inter-module connections originate only from the excitatory

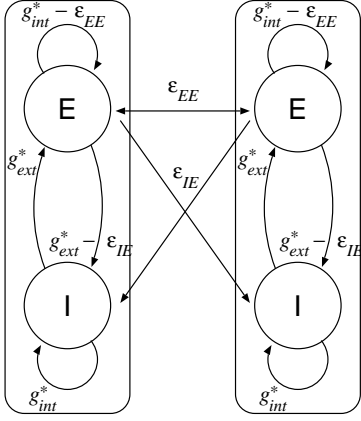


Figure 4: Arrangement of the connection strengths in the two-module system that results in the inter-module synchronization of chaotic firings.

ensembles, namely, $\epsilon_{EI} = \epsilon_{II} = 0$, because the inter-columnar long-range connections in the cortex are excitatory [Gilbert & Wiesel, 1983; Ts'o et al., 1986].

According to Appendix B, let us introduce two vectors \mathbf{x}_1 and \mathbf{x}_2 , each of which describes the average dynamics of the neurons in the respective module. In the above arrangement of connections, the two-module system has a synchronized solution $\mathbf{x}_1 = \mathbf{x}_2$, and this synchronized solution shows a chaotic attractor characterized by the one-module system with g_{int}^* and g_{ext}^* . As shown later, the stability of this synchronized solution depends on the inter-module connection strength ϵ_{IE} . Let us fix the values of the parameters at $D = 0.0042$, $g_{int}^* = 4$, $g_{ext}^* = 2.8$, and $\epsilon_{EE} = 0.4$, and examine whether the stability of the synchronized solution depends on ϵ_{IE} . The change in $J_{E_1} - J_{E_2}$ over time for $\epsilon_{IE} = 0.84$ and $\epsilon_{IE} = 0.835$ is shown in Figs. 5(a) and 5(b), respectively. Note that J_{E_k} denotes the firing rate (probability flux) of the excitatory ensemble in the k -th module. It is observed that the synchronized solution $\mathbf{x}_1 = \mathbf{x}_2$ is stable for $\epsilon_{IE} = 0.84$, and that intermittent behavior typical of on-off intermittency [Fujisaka & Yamada, 1986; Heagy *et al.*, 1994; Ott & Sommerer, 1994; Hata & Miyazaki, 1997] appears for $\epsilon_{IE} = 0.835$. As shown in Fig. 5(b), there exist nearly synchronized states where $J_{E_1} \sim J_{E_2}$ between the intermittent bursts, and they are called laminar states. The distribution of the duration of the laminar states is shown in Fig. 6, and a slope of $\sim \tau^{-1.5}$ which is typical of on-off intermittency [Heagy *et al.*, 1994; Hata & Miyazaki, 1997] is observed. A laminar state was defined as a state that satisfies $J_{E_1} - J_{E_2} < h$ where h is an arbitrary threshold. It is also observed that the slope does not depend on the threshold h .

To examine the stability of the synchronized solution $\mathbf{x}_1 = \mathbf{x}_2$, the transverse Lyapunov exponent λ_{\perp} of the synchronized solution $\mathbf{x}_1 = \mathbf{x}_2$ was numerically calculated by the method shown in Appendix C, and its dependence on ϵ_{IE} is shown in Fig. 7. It is observed that

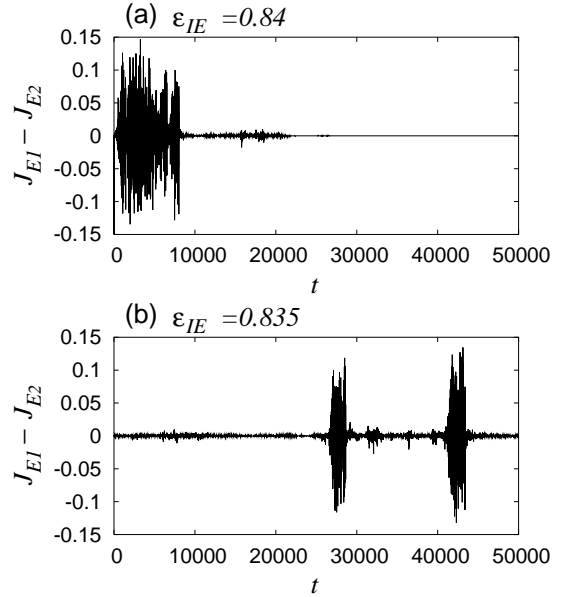


Figure 5: Change in $J_{E_1} - J_{E_2}$ over time in a two-module system where (a) $\epsilon_{IE} = 0.84$ and (b) $\epsilon_{IE} = 0.835$. The other parameters are fixed at $D = 0.0042$, $g_{int}^* = 4$, $g_{ext}^* = 2.8$, and $\epsilon_{EE} = 0.4$.

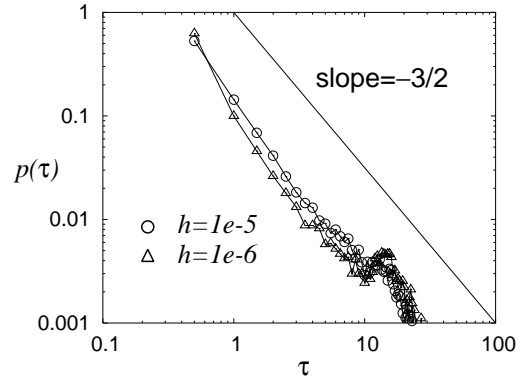


Figure 6: Distribution $p(\tau)$ of the duration τ of the laminar state for $D = 0.0042$, $g_{int}^* = 4$, $g_{ext}^* = 2.8$, $\epsilon_{EE} = 0.4$, and $\epsilon_{IE} = 0.835$. A slope of $\sim \tau^{-1.5}$ which is typical of on-off intermittency, is observed independent of the threshold h .

as ϵ_{IE} increases, λ_{\perp} decreases, and λ_{\perp} takes the value of zero when $\epsilon_{IE} = \epsilon_0 \sim 0.835$. The synchronized state is stable for $\epsilon_{IE} > \epsilon_0$ because $\lambda_{\perp} < 0$, while it is unstable for $\epsilon_{IE} < \epsilon_0$ because $\lambda_{\perp} > 0$. Such destabilization of the invariant manifold $\mathbf{x}_1 = \mathbf{x}_2$ along the direction transverse to this manifold is called blowout bifurcation [Ott & J.C. Sommerer, 1994].

Although the above results were obtained in the two-module system consisting of infinite neurons, similar phenomena are observed in the two-module system with a finite number of neurons. The on-off intermittency

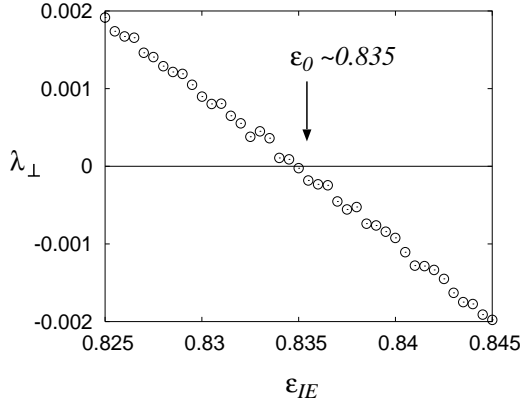


Figure 7: Dependence of the transverse Lyapunov exponent λ_{\perp} of the synchronized solution $\mathbf{x}_1 = \mathbf{x}_2$ on ϵ_{IE} where $D = 0.0042$, $g_{int}^* = 4$, $g_{ext}^* = 2.8$, and $\epsilon_{EE} = 0.4$.

observed in the two-module system with $N_{E_k} = N_{I_k} = 5000$ is shown in Fig. 8. The firing times of the excitatory neurons are plotted in Fig. 8(a), and it is observed that the inter-module synchronization is intermittently broken. The difference in the average firing rate J_{E_k} of two excitatory ensembles is shown in Fig. 8(b). Note

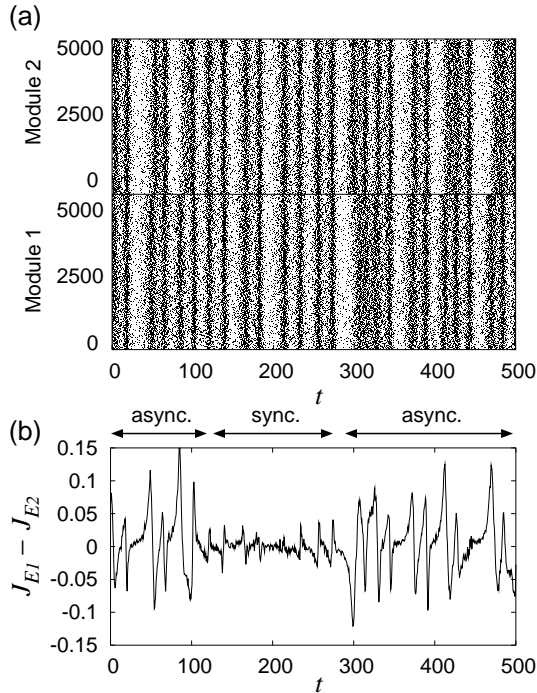


Figure 8: On-off intermittency observed in the two-module system with $N_{E_k} = N_{I_k} = 5000$. (a) Raster plot of the firing times of the excitatory neurons. (b) Difference in the average firing rate J_{E_k} of the neurons in the excitatory ensembles of the two modules. The parameters are identical with those in Fig. 5(b).

that J_{E_k} is defined as

$$J_{X_k}(t) \equiv \frac{1}{N_{X_k} d} \sum_{i=1}^{N_{X_k}} \sum_j \Theta(t - t_j^{(i)}), \quad (10)$$

$$\Theta(t) = \begin{cases} 1 & \text{for } 0 \leq t < d \\ 0 & \text{otherwise} \end{cases}, \quad (11)$$

where $t_j^{(i)}$ is the j -th firing time of the i -th excitatory neuron in the k -th ensemble X_k ($X = E$ or I) and $d = 1.0$.

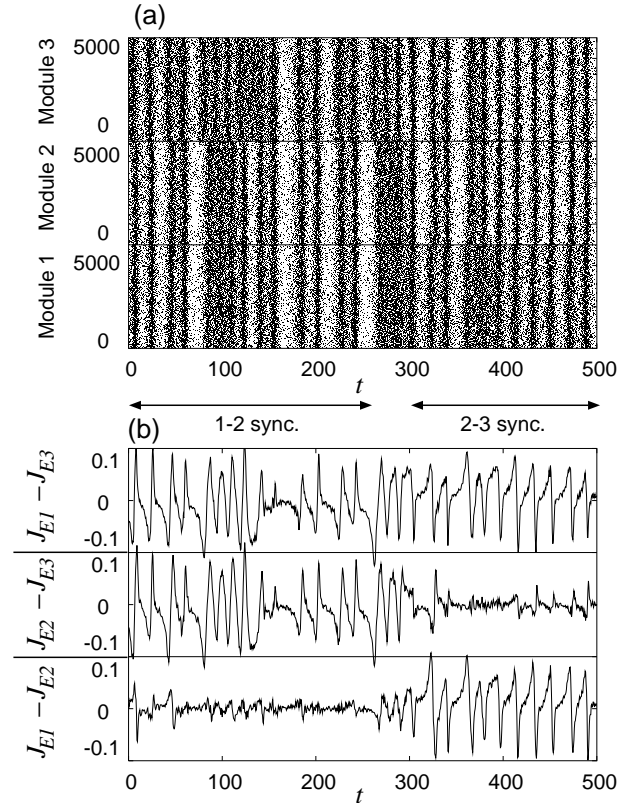


Figure 9: Chaotic itinerancy in the three-module system where $N_{E_k} = N_{I_k} = 5000$ and $g_{int}^* = 4$, $g_{ext}^* = 2.8$, $\epsilon_{EE} = 0.4$, $\epsilon_{IE} = 0.65$, $g_{EE} = g_{int}^* - 2\epsilon_{EE}$, $g_{II} = g_{int}^*$, $g_{IE} = g_{ext}^* - 2\epsilon_{IE}$, and $g_{EI} = g_{ext}^*$. (a) Raster plot of the firing times of the excitatory neurons in the three modules. (b) Change in the difference in the average firing rate of the excitatory neurons J_{E_k} over time.

Such intermittent behavior can induce chaotic itinerancy, which is an example of high-dimensional chaos, in the M -module system. The chaotic itinerancy in the three-module system with $N_{E_k} = N_{I_k} = 5000$ is shown in Fig. 9. The intra-module connections are defined as $g_{EE} = g_{int}^* - 2\epsilon_{EE}$, $g_{II} = g_{int}^*$, $g_{IE} = g_{ext}^* - 2\epsilon_{IE}$, and $g_{EI} = g_{ext}^*$. It is observed that modules 1 and 2 are synchronized during $0 \leq t \leq 200$, and modules 2 and 3 are synchronized during $250 \leq t \leq 500$. In other words, synchronized pairs are rearranged chaotically. Such dynamical rearrangement of synchronized clusters might be

related to dynamical cell assembly [Hebb, 1949; Fujii *et al.*, 1996] and transitions of memory states in associative memory models [Aoyagi & Aoki, 2004].

4 Tests on Morris-Lecar Neurons

The above results were obtained using the canonical model of slowly connected class 1 neurons [Izhikevich, 1999, 2000]. We found that similar results were observed in networks of other class 1 neurons. Let us consider a network of non-dimensional Morris-Lecar neurons [Ermentrout, 1996].

The M -module system that is composed of non-dimensional Morris-Lecar neurons is defined as

$$\begin{aligned} \dot{V}_{E_k}^{(i)} &= -g_L(V_{E_k}^{(i)} - V_L) - g_K w_{E_k}^{(i)}(V_{E_k}^{(i)} - V_K) \\ &\quad - g_{Ca} m_\infty(V_{E_k}^{(i)})(V_{E_k}^{(i)} - V_{Ca}) \\ &\quad + H_{E_k} + \xi_{E_k}^{(i)}(t) \\ &\quad + g_{E_k E_k} I_{E_k}(t) - g_{E_k I_k} I_{I_k}(t) \\ &\quad + \sum_{l \neq k} (\epsilon_{E_k E_l} I_{E_l}(t) - \epsilon_{E_k I_l} I_{I_l}(t)), \end{aligned} \quad (12)$$

$$\begin{aligned} \dot{w}_{E_k}^{(i)} &= \lambda(V_{E_k}^{(i)})(w_\infty(V_{E_k}^{(i)}) - w_{E_k}^{(i)}), \\ \dot{V}_{I_k}^{(i)} &= -g_L(V_{I_k}^{(i)} - V_L) - g_K w_{I_k}^{(i)}(V_{I_k}^{(i)} - V_K) \\ &\quad - g_{Ca} m_\infty(V_{I_k}^{(i)})(V_{I_k}^{(i)} - V_{Ca}) \\ &\quad + H_{I_k} + \xi_{I_k}^{(i)}(t) \\ &\quad + g_{I_k E_k} I_{E_k}(t) - g_{I_k I_k} I_{I_k}(t) \\ &\quad + \sum_{l \neq k} (\epsilon_{I_k E_l} I_{E_l}(t) - \epsilon_{I_k I_l} I_{I_l}(t)), \end{aligned} \quad (13)$$

$$\begin{aligned} \dot{w}_{I_k}^{(i)} &= \lambda(V_{I_k}^{(i)})(w_\infty(V_{I_k}^{(i)}) - w_{I_k}^{(i)}), \\ I_X(t) &= \frac{1}{N_X} \sum_{i=1}^{N_X} \sum_j \frac{1}{\kappa_X} \exp\left(-\frac{t - t_j^{(i)}}{\kappa_X}\right), \\ m_\infty(V) &= 0.5(1 + \tanh((V - V_1)/V_2)), \\ w_\infty(V) &= 0.5(1 + \tanh((V - V_3)/V_4)), \\ \lambda(V) &= \frac{1}{3} \cosh((V - V_3)/(2V_4)), \\ \langle \xi_X^{(i)}(t) \xi_Y^{(j)}(t') \rangle &= D \delta_{XY} \delta_{ij} \delta(t - t'), \\ X, Y &= E_k \text{ or } I_k (k = 1, 2, \dots, M). \end{aligned} \quad (14)$$

$$\dot{w}_{I_k}^{(i)} = \lambda(V_{I_k}^{(i)})(w_\infty(V_{I_k}^{(i)}) - w_{I_k}^{(i)}), \quad (15)$$

$$I_X(t) = \frac{1}{N_X} \sum_{i=1}^{N_X} \sum_j \frac{1}{\kappa_X} \exp\left(-\frac{t - t_j^{(i)}}{\kappa_X}\right), \quad (16)$$

$$m_\infty(V) = 0.5(1 + \tanh((V - V_1)/V_2)), \quad (17)$$

$$w_\infty(V) = 0.5(1 + \tanh((V - V_3)/V_4)), \quad (18)$$

$$\lambda(V) = \frac{1}{3} \cosh((V - V_3)/(2V_4)), \quad (19)$$

$$\langle \xi_X^{(i)}(t) \xi_Y^{(j)}(t') \rangle = D \delta_{XY} \delta_{ij} \delta(t - t'), \quad (20)$$

$$X, Y = E_k \text{ or } I_k (k = 1, 2, \dots, M). \quad (21)$$

The Morris-Lecar neuron is a simplified model of the class 1 Connor model and the class 2 Hodgkin-Huxley model, and it shows the behavior of a class 1 neuron or a class 2 neuron depending on the values of the parameters. We choose values for the parameters that result in class 1 behavior, namely, $g_L = 0.5$, $g_K = 2$, $g_{Ca} = 1.33$, $V_L = -0.5$, $V_K = -0.7$, $V_{Ca} = 1$, $V_1 = -0.01$, $V_2 = 0.15$, $V_3 = 0.1$, and $V_4 = 0.145$. H_{E_k} and H_{I_k} are the external constant inputs, and, for a single Morris-Lecar neuron with the above values for the parameters, saddle-node-on-limit-cycle bifurcation takes place at $H_{E_k}, H_{I_k} = H_0 \sim 0.0691$, and this neuron starts to

oscillate when $H_{E_k}, H_{I_k} > H_0$. In the following, we use $H_{E_k} = H_{I_k} = 0.068$. The synaptic time constant κ_X is fixed at $\kappa_X = 6$ for all ensembles. The firing time of the i -th neuron in ensemble X is defined as the time at which $w_X^{(i)}$ exceeds 0.25.

First, let us consider a one-module system. Upon selection of appropriate values for the parameters, chaotic dynamics similar to the dynamics shown in Fig. 2 appear. The chaotic attractor observed in a one-module

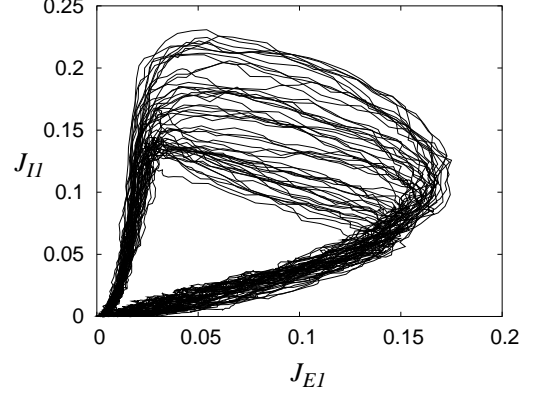


Figure 10: Chaotic attractor observed in the one-module system of Morris-Lecar neurons with $N_{E_1} = N_{I_1} = 5000$ where $D = 6 \times 10^{-5}$, $g_{int} = 0.7$, and $g_{ext} = 0.49$.

system of Morris-Lecar neurons with $N_{E_1} = N_{I_1} = 5000$ and where $D = 6 \times 10^{-5}$, $g_{int} = 0.7$, and $g_{ext} = 0.49$, is shown in Fig. 10, in which the average firing rates J_{E_1} and J_{I_1} were calculated by Eq. (10). Note that this

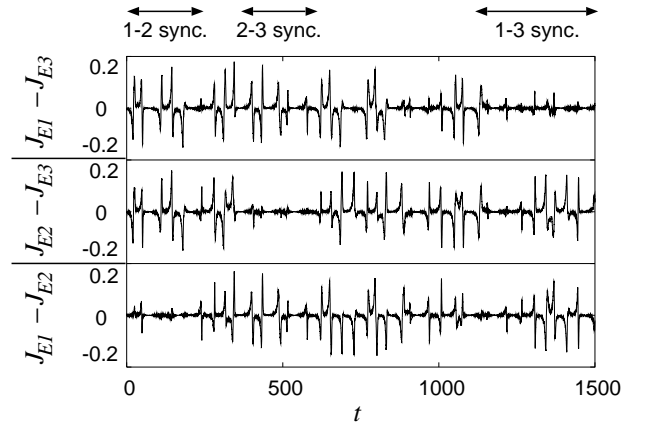


Figure 11: Chaotic itinerancy in a three-module system of Morris-Lecar neurons. Changes in the difference in the average firing rate J_{E_k} of excitatory neurons in the three modules over time are shown. Similar to the canonical model, for the inter-module connections $\epsilon_{EE} = 0.07$ and $\epsilon_{IE} = 0.15$, the intra-module connection strengths were set at $g_{EE} = g_{int}^* - 2\epsilon_{EE}$, $g_{II} = g_{int}^*$, $g_{IE} = g_{ext}^* - 2\epsilon_{IE}$, and $g_{EI} = g_{ext}^*$ where $g_{int}^* = 0.7$ and $g_{ext}^* = 0.49$.

chaotic attractor is observed in the one-module system

in the case where the ratio of g_{ext} to g_{int} is 0.7, which is identical with the ratio in the canonical model in Fig. 2.

The chaotic itinerancy in a three-module system of Morris-Lecar neurons is shown in Fig. 11. Similar to the canonical model, the intra-module connection strengths are set as $g_{EE} = g_{int}^* - 2\epsilon_{EE}$, $g_{II} = g_{int}^*$, $g_{IE} = g_{ext}^* - 2\epsilon_{IE}$, and $g_{EI} = g_{ext}^*$ where $g_{int}^* = 0.7$ and $g_{ext}^* = 0.49$. It is observed that the synchronized clusters are also chaotically rearranged in the network of Morris-Lecar neurons.

5 Discussion and Conclusions

To elucidate the mechanism by which high-dimensional chaos emerges in neural systems, the synchronization of chaotic firings in class 1 pulse neural networks with excitatory and inhibitory ensembles was analyzed.

In a network consisting of a single module, linear analyses around the equilibrium points with the Fokker-Planck equation were performed, and various synchronized firings were observed depending on the values of the parameters such as the noise intensity and the connection strengths. We focused on the synchronized chaotic firings, in which the interval of the synchronized firings fluctuated chaotically, and we observed a low-dimensional chaotic attractor in the limit of a large number of neurons.

Next, to elucidate the mechanism by which high-dimensional chaos emerges in neural systems, we examined the inter-module synchronization of chaotic firings in a system with two modules. Because the connections between neurons are not diffusive but instead are synaptic with chemical synapses, the inter-module synchronization of chaotic firings was not stable when the two modules were connected without modifying the connection strengths. Thus, we introduced an arrangement of connection strengths such that the inter-module synchronization of chaotic firings would become a solution of the system. With such connections, when the inter-module connection strengths were large, it was found that the inter-module synchronization of chaotic firings was stable, and when the inter-module connection strengths were reduced, the inter-module synchronization of chaotic firings became unstable due to blowout bifurcation [Ott & Sommerer, 1994]. A behavior typical of on-off intermittency [Fujisaka & Yamada, 1986; Heagy *et al.*, 1994; Hata & Miyazaki, 1997] was also observed. When the inter-module synchronization of chaotic firings was stable, the system was confined to a low-dimensional chaotic attractor, and when this attractor became unstable by blowout bifurcation, the system was blown out from the vicinity of the low-dimensional invariant manifold. In other words, a transition from low-dimensional chaos to high-dimensional chaos took place. Blowout bifurcation may induce chaotic itinerancy, which is often observed in high-dimensional chaotic systems. To confirm this, we studied a three-module system, and it was

observed that the synchronized clusters were rearranged chaotically.

Because the above results were obtained using the canonical model of slowly connected class 1 neurons [Izhikevich, 1999, 2000], we studied whether similar results are observed in a network of other class 1 neurons. In the network of Morris-Lecar neurons which are a model of class 1 neurons, synchronization of chaos and chaotic rearrangement of synchronized clusters were observed.

If high-dimensional chaos exists in biological systems, it might play an important role in information processing in the brain, as has been proposed in modeling studies [Aihara *et al.*, 1990; Inoue & Nagayoshi, 1991; Nara & Davis, 1992; Tsuda, 1992; Adachi & Aihara, 1997; Uchiyama & Fujisaka, 2004]. The synchronization of chaos and its destabilization which were observed in our model, may be one of the mechanisms by which high-dimensional chaos is generated in neural systems.

Chaotic itinerancy in pulse neural networks was previously reported in networks of four or five Bonhöffer-van der Pol neurons by Tsumoto *et al.* [2002], and they stated that the range of values for the parameters that resulted in chaotic itinerancy was very narrow in their model. On the other hand, in our model, the range of values for the parameters that results in chaotic itinerancy, is wide because it is easy to find blowout bifurcation in the two-module system when intra-module synchronized chaotic firings exist in each module. Moreover, such phenomena can be observed even in a noisy environment because synchronized chaotic firings are realized by the noise-induced bifurcation in our model.

Finally, we assumed that the properties of the neurons and connections were uniform in a module. Of course, such model is a rough estimation of the brain where various types of neurons exist and the connections between them are not uniform. It is known that the heterogeneity of the system causes various interesting phenomena such as traveling waves and enhancement of temporal periodicity [Zhou *et al.*, 2001; Wright *et al.*, 2004]. Thus, when such heterogeneity is introduced into our model, more complex dynamics are expected and they will be the subject of future studies.

A The Fokker-Planck Equation for the One-Module System

To analyze the dynamics of the one-module system, we use the Fokker-Planck equations [Kuramoto, 1984; Gerstner & Kistler, 2002] which are written as

$$\begin{aligned} \frac{\partial n_E}{\partial t} &= -\frac{\partial}{\partial \theta_E}(A_E n_E) \\ &\quad + \frac{D}{2} \frac{\partial}{\partial \theta_E} \left\{ B_E \frac{\partial}{\partial \theta_E} (B_E n_E) \right\}, \quad (22) \\ \frac{\partial n_I}{\partial t} &= -\frac{\partial}{\partial \theta_I}(A_I n_I) \end{aligned}$$

$$+ \frac{D}{2} \frac{\partial}{\partial \theta_I} \left\{ B_I \frac{\partial}{\partial \theta_I} (B_I n_I) \right\}, \quad (23)$$

$$A_E(\theta_E, t) = (1 - \cos \theta_E) + (1 + \cos \theta_E) \\ \times (r_E + g_{EE} I_E(t) - g_{EI} I_I(t)), \quad (24)$$

$$A_I(\theta_I, t) = (1 - \cos \theta_I) + (1 + \cos \theta_I) \\ \times (r_I + g_{IE} I_E(t) - g_{II} I_I(t)), \quad (25)$$

$$B_E(\theta_E, t) = 1 + \cos \theta_E, \quad (26)$$

$$B_I(\theta_I, t) = 1 + \cos \theta_I, \quad (27)$$

for the normalized number densities of excitatory and inhibitory neurons, in which

$$n_E(\theta_E, t) \equiv \frac{1}{N_E} \sum_{i=1}^{N_E} \delta(\theta_E^{(i)} - \theta_E), \quad (28)$$

$$n_I(\theta_I, t) \equiv \frac{1}{N_I} \sum_{i=1}^{N_I} \delta(\theta_I^{(i)} - \theta_I), \quad (29)$$

in the limit of $N_E, N_I \rightarrow \infty$. The probability flux for each ensemble is defined as

$$J_E(\theta_E, t) = A_E n_E - \frac{D}{2} B_E \frac{\partial}{\partial \theta_E} (B_E n_E), \quad (30)$$

$$J_I(\theta_I, t) = A_I n_I - \frac{D}{2} B_I \frac{\partial}{\partial \theta_I} (B_I n_I), \quad (31)$$

respectively. In the limit of $N_X \rightarrow \infty$, $I_X(t)$ in Eq. (3) follows a differential equation that is written as

$$I_X \dot{=} - \frac{1}{\kappa_X} \left(I_X(t) - \frac{1}{2} J_X(t) \right), \quad (32)$$

where $J_X(t) \equiv J_X(\pi, t)$ is the probability flux at $\theta_X = \pi$.

By integrating the Fokker-Planck equations (22) and (23) and the differential equation (32) simultaneously, the dynamics of the network that is governed by Eqs. (1) and (2) can be analyzed.

B Numerical Integration of the Fokker-Planck Equations

In this section, we provide a method of performing the numerical integration of the Fokker-Planck equations (22) and (23). Because the normalized number densities given by Eqs. (28) and (29) are 2π -periodic functions of θ_E and θ_I , respectively, they can be expanded as

$$n_E(\theta_E, t) = \frac{1}{2\pi} + \sum_{k=1}^{\infty} (a_k^E(t) \cos(k\theta_E) + b_k^E(t) \sin(k\theta_E)),$$

$$n_I(\theta_I, t) = \frac{1}{2\pi} + \sum_{k=1}^{\infty} (a_k^I(t) \cos(k\theta_I) + b_k^I(t) \sin(k\theta_I)),$$

and, by substituting them, Eqs. (22) and (23) are transformed into a set of ordinary differential equations of a_k^X

and b_k^X , which are written as

$$\frac{da_k^{(X)}}{dt} = -(r_X + K_X + 1) k b_k^{(X)} \\ - (r_X + K_X - 1) \frac{k}{2} (b_{k-1}^{(X)} + b_{k+1}^{(X)}) \\ - \frac{Dk}{8} g(a_k^{(X)}), \quad (35)$$

$$\frac{db_k^{(X)}}{dt} = (r_X + K_X + 1) k a_k^{(X)} \\ + (r_X + K_X - 1) \frac{k}{2} (a_{k-1}^{(X)} + a_{k+1}^{(X)}) \\ - \frac{Dk}{8} g(b_k^{(X)}) \quad (36)$$

$$g(x_k) = (k-1)x_{k-2} + 2(2k-1)x_{k-1} + 6kx_k \\ + 2(2k+1)x_{k+1} + (k+1)x_{k+2}, \quad (37)$$

$$K_X \equiv g_{XE} I_E - g_{XI} I_I, \quad (38)$$

$$a_0^{(X)} \equiv \frac{1}{\pi}, \quad (39)$$

$$b_0^{(X)} \equiv 0, \quad (40)$$

where $X = E$ or I . Using a vector $\mathbf{x} = (I_E, I_I, a_1^E, b_1^E, a_1^I, b_1^I, a_2^E, b_2^E, a_2^I, b_2^I, \dots)^t$, the ordinary differential equation $\dot{\mathbf{x}} = \mathbf{f}(\mathbf{x})$ is defined by (32), (35), and (36). By integrating this ordinary differential equation numerically, the time series of the probability fluxes J_E and J_I are obtained. For numerical calculations, each Fourier series is truncated at the first 40 or 60 terms.

The bifurcation lines of the Hopf bifurcation and the saddle-node bifurcation in Fig. 1 were obtained as follows. A stationary solution \mathbf{x}_s was numerically obtained by the Newton method [Press *et al.* 1988], and the eigenvalues of the Jacobian matrix $D\mathbf{f}(\mathbf{x}_s)$ that had been numerically obtained by using the QR algorithm [Press *et al.* 1988], were examined to find the bifurcation lines. On the other hand, the bifurcation lines of the homoclinic bifurcation were obtained by observing the long-time behaviors of the solutions of $\dot{\mathbf{x}} = \mathbf{f}(\mathbf{x})$.

The largest Lyapunov exponent in Fig. 3 was calculated by the standard technique [Ott, 1993], namely, by calculating the expansion rate of two nearby trajectories, each of which follows $\dot{\mathbf{x}} = \mathbf{f}(\mathbf{x})$.

C Numerical Calculation of the Transverse Lyapunov Exponent

Let us consider a two-module system characterized by two vectors \mathbf{x}_1 and \mathbf{x}_2 (as defined in Appendix B), and define a mean vector \mathbf{X} and a difference vector $\Delta\mathbf{x}$ as

$$\mathbf{X} = \frac{\mathbf{x}_1 + \mathbf{x}_2}{2}, \quad (41)$$

$$\Delta\mathbf{x} = \frac{\mathbf{x}_1 - \mathbf{x}_2}{2}. \quad (42)$$

When the two modules are synchronized ($\mathbf{x}_1 = \mathbf{x}_2$), the mean vector \mathbf{X} moves on a chaotic attractor that is restricted to the invariant manifold $\Delta\mathbf{x} = 0$. The transverse stability of the synchronized solution is determined by the transverse Lyapunov exponent λ_{\perp} , which is defined by

$$\lambda_{\perp} = \lim_{n \rightarrow \infty} \frac{1}{n\tau} \sum_{j=1}^n \ln \left(\frac{|\Delta\mathbf{x}(t+j\tau)|}{|\Delta\mathbf{x}(t+(j-1)\tau)|} \right), \quad (43)$$

where τ is an arbitrary short period of time. When the synchronized solution $\mathbf{x}_1 = \mathbf{x}_2$ is unstable, the components of the vector $\Delta\mathbf{x}$ exponentially grow and take large values. Thus, the length of $\Delta\mathbf{x}$ should be periodically normalized to the value l based on the equations

$$\mathbf{x}'_1 = \mathbf{X} + l \frac{\Delta\mathbf{x}}{|\Delta\mathbf{x}|}, \quad (44)$$

$$\mathbf{x}'_2 = \mathbf{X} - l \frac{\Delta\mathbf{x}}{|\Delta\mathbf{x}|}. \quad (45)$$

Acknowledgement

This research was partially supported by a Grant-in-Aid for Encouragement of Young Scientists (B) (No. 17700226) from the Ministry of Education, Culture, Sports, Science, and Technology, Japan.

References

- Adachi, M. & Aihara, K. [1997] "Associative dynamics in a chaotic neural network," *Neural Network* **10**, 83–98.
- Aihara, K., Takabe, T., & Toyoda, M. [1990] "Chaotic neural networks," *Phys. Lett. A* **144**, 333–340.
- Aoyagi, T. & Aoki, T. [2004] "Possible role of synchronous input spike trains in controlling the function of neural networks," *Neurocomput.* **58-60**, 259–264.
- Elson, R. C., Selverston, A. I., Huerta, R., Rulkov, N. F., Rabinovich, M. I., & Abarbanel, D. I. [1998] "Synchronous behavior of two coupled biological neurons," *Phys. Rev. Lett.* **81**, 5692–5695.
- Ermentrout, B. [1996] "Type I membranes, phase resetting curves, and synchrony," *Neural Comput.* **8**, 979–1001.
- Feudel, U., Neiman, A., Pei, X., Wijtenek, W., Braun, H., Huber, M., & Moss, F. [2000] "Homoclinic bifurcation in a Hodgkin-Huxley model of thermally sensitive neurons," *Chaos* **10**, 231–239.
- Freeman, W. J. [1987] "Simulation of chaotic EEG patterns with a dynamic model of the olfactory system," *Biol. Cybern.* **56**, 139–150.
- Fujii, H., Ito, H., Aihara, K., Ichinose, N., & Tsukada, M. [1996] "Dynamical cell assembly hypothesis – Theoretical possibility of spatio-temporal coding in the cortex," *Neural Networks* **9**, 1303–1350.
- Fujisaka, H. & Yamada, T. [1986] "Stability theory of synchronized motion in coupled-oscillator systems. IV," *Prog. Theor. Phys.* **75**, 1087–1104.
- Gerstner, W. & Kistler, W. [2002] *Spiking Neuron Models* (Cambridge Univ. Press, Cambridge).
- Gilbert, C. D. & Wiesel, T. N. [1983] "Clustered intrinsic connections in cat visual cortex," *J. Neurosci.* **3**, 1116–1133.
- Hata, H. & Miyazaki, S. [1997] "Exactly solvable maps of on-off intermittency," *Phys. Rev. E* **55**, 5311–5314.
- Hayashi, H., Ishizuka, S., Ohta, M., & Hirakawa, K. [1982] "Chaotic behavior in the onchidium giant neuron under sinusoidal stimulation," *Phys. Lett.* **88A**, 435–438.
- Heagy, J. F., Platt, N., & Hammel, S. M. [1994] "Characterization of on-off intermittency," *Phys. Rev. E* **49**, 1140–1150.
- Hebb, D. O. [1949] *The Organization of Behavior – a neuropsychological theory* (John Wiley, New York).
- Inoue, M. & Nagayoshi, A. [1991] "A chaos neuro-computer," *Phys. Lett. A* **158**, 373–376.
- Izhikevich, E. M. [1999] "Class 1 neural excitability, conventional synapses, weakly connected networks, and mathematical foundations of pulse-coupled models," *IEEE Trans. Neural Networks* **10**, 499–507.
- Izhikevich, E. M. [2000] "Neural excitability, spiking and bursting," *Int. J. Bifurcation and Chaos* **10**, 1171–1266.
- Kanamaru, T. & Sekine, M. [2003] "Array-enhanced coherence resonance in the diffusively coupled active rotators and its analysis with the nonlinear Fokker-Planck equation," *IEICE Trans. on Fundamentals* **E86-A**, 2197–2202.
- Kanamaru, T. & Sekine, M. [2005] "Synchronized firings in the networks of class 1 excitable neurons with excitatory and inhibitory connections and their dependences on the forms of interactions," *Neural Comput.* **17**, 1315–1338.

- Kaneko, K. & Tsuda, I. [2000] *Complex Systems: Chaos and beyond, a constructive approach with applications in life sciences* (Springer-Verlag, Berlin).
- Kuramoto, Y. [1984] *Chemical oscillations, waves, and turbulence* (Springer, Berlin).
- Lindner, B., Garía-Ojalvo, J., Neiman, A., & Schimansky-Geier, L. [2004] “Effects of noise in excitable systems,” *Physics Reports* **392**, 321–424.
- Matsumoto, G., Aihara, K., Ichikawa, M., & Tasaki, A. [1984] “Periodic and nonperiodic responses of membrane potentials in squid giant axons during sinusoidal current stimulation,” *J. Theoret. Neurobiol.* **3**, 1–14.
- Nara, S. & Davis, P. [1992] “Chaotic wandering and search in a cycle-memory neural network,” *Prog. Theor. Phys.* **88**, 845–855.
- Nicholls, J. G., Martin, A. R., Wallace, B. G., & Fuchs, P. A. [2001] *From Neuron to Brain* (Sinauer Associates Inc. Publishers, Massachusetts).
- Ott, E. [1993] *Chaos in Dynamical Systems* (Cambridge University Press, New York).
- Ott, E. & Sommerer, J. C. [1994] “Blowout bifurcations: the occurrence of riddled basins and on-off intermittency,” *Phys. Lett. A* **188**, 39–47.
- Pikovsky, A. S. & Kurth, J. [1997] “Coherence resonance in a noise-driven excitable system,” *Phys. Rev. Lett.* **78**, 775–778.
- Press, W. H., Flannery, B. P., Teukolsky, S. A., & Vetterling, W. T. [1988] *Numerical Recipes in C* (Cambridge Univ. Press, New York).
- Ts’o, D. Y., Gilbert, C. D., & Wiesel, T. N. [1986] “Relationships between horizontal interactions and functional architecture in cat striate cortex as revealed by cross-correlation analysis,” *J. Neurosci.* **6**, 1160–1170.
- Tsuda, I. [1992] “Dynamic link of memory – Chaotic memory map in nonequilibrium neural networks,” *Neural Networks* **5**, 313–326.
- Tsumoto, K., Yoshinaga, T., & Kawakami, H. [2002] “Bifurcations of synchronized responses in synaptically coupled Bonhöffer-van der Pol neurons,” *Phys. Rev. E* **65**, 036230.
- Uchiyama, S. & Fujisaka, H. [2004] “Chaotic itinerancy in the oscillator neural network without Lyapunov functions,” *Chaos* **14**, 699–706.
- Varona, P., Torres, J. J., Huerta, R., Abarbanel, H. D. I., & Rabinovich, M. I. [2001] “Regularization mechanism of spiking-bursting neurons,” *Neural Networks* **14**, 865–875.
- van Vreeswijk, C. & Sompolinsky, H. [1996] “Chaos in neuronal networks with balanced excitatory and inhibitory activity,” *Science* **274**, 1724–1726.
- Wright, J. J., Rennie, C. J., Lees, G. J., Robinson, P.A., Bourke, P. D., Chapman, C. L., Gordon, E., & Rowe, D. L. [2004] “Simulated electrocortical activity at microscopic, mesoscopic, and global scales,” *Int. J. Bifurcation and Chaos* **14**, 853–872.
- Yoshioka, M. [2005] “Chaos synchronization in gap-junction-coupled neurons,” *Phys. Rev. E* **71**, 065203(R).
- Zaks, M. A., Sailer, X., Schimansky-Geier, L., & Neiman, A. B. [2005] “Noise induced complexity: From subthreshold oscillations to spiking in coupled excitable systems,” *Chaos* **15**, 026117.
- Zhou, C., Kurth, J., & Hu, B. [2001] “Array-enhanced coherence resonance: nontrivial effects of heterogeneity and spatial independence of noise,” *Phys. Rev. Lett.* **87**, 098101.